A large area TOF-tracker device based on multi-gap Resistive Plate Chambers

Published by IOP Publishing for Sissa Medialab
Received: *June 9, 2016*
Accepted: *September 30, 2016*
Published: *October 5, 2016*

13th Workshop on Resistive Plate Chambers and Related Detectors,
22–26 February 2016,
Ghent, Belgium

A large area TOF-tracker device based on multi-gap Resistive Plate Chambers

P. Assis,[a,b] **A. Bernardino,**[a] **A. Blanco,**[a,1] **F. Clemêncio,**[c,d] **N. Carolino,**[a] **O. Cunha,**[a] **M. Ferreira,**[a] **P. Fonte,**[a,e] **L. Lopes,**[a] **C. Loureiro,**[c] **R. Luz,**[a,b] **L. Mendes,**[a] **J. Michel,**[f] **A. Neiser,**[g] **A. Pereira,**[a] **M. Pimenta,**[a,b] **R. Shellard**[h] **and M. Traxler**[g]

[a] *LIP, Laboratório de Instrumentação e Física Experimental de Partículas, Portugal*
[b] *Instituto Superior Técnico - IST, Universidade de Lisboa, Lisboa, Portugal*
[c] *LIBPhys, Department of Physics, University of Coimbra, Coimbra, Portugal*
[d] *Escola Superior de Tecnologia da Saúde do Porto - IPP, Vila Nova de Gaia, Portugal*
[e] *Instituto Superior de Engenharia de Coimbra, Coimbra, Portugal*
[f] *Institut für Kernphysik, Goethe-Universität, Frankfurt, Germany*
[g] *GSI Helmholtz Centre for Heavy Ion Research, Darmstadt, Germany*
[h] *Centro Brasileiro de Pesquisas Físicas - CBPF, Brazil*

E-mail: alberto@coimbra.lip.pt

Abstract: The TOF-tracker concept, the simultaneous measurement of accurate time and bi-dimensional space coordinates in a single gaseous detector, has been previously demonstrated. The detector yielded a time resolution of 77 ps σ along with a bi-dimensional position resolution of 38 μm σ over a full active area of $60 \times 60\,\mathrm{mm}^2$. In here, we report about a large area, $1550 \times 1250\,\mathrm{mm}^2$, TOF-tracker device, tested by tracking cosmic muons, yielding a position resolution down to 1.33 mm σ, a simultaneous time resolution of 150 ps σ and 92% detection efficiency, over the entire area of the detector. The sub-millimetre electronic resolution of the readout chain suggests that the position resolution here reported could be dominated by non-corrected systematic effects and therefore it could be yet significantly improved.

Keywords: Instrumentation and methods for time-of-flight (TOF) spectroscopy; Particle detectors; Particle tracking detectors (Gaseous detectors); Resistive-plate chambers

[1] Corresponding author.

doi:10.1088/1748-0221/11/10/C10002

2016 JINST 11 C10002

Contents

1 Introduction

The particle identification [1] by time-of-flight technique [2] relies on the accurate measurement of the flight path by tracking detectors and on the measurement of the flight time by dedicated start and stop detectors. These tasks are normally performed by detectors specialized for each task, but there are advantages (i.e. reduced costs, less extension of the experimental set-up) in doing the measurements by detectors capable of performing both tasks simultaneously. Each particle would be measured several times, improving timing accuracy, without the need for an external reference timing detector. The tracking would be performed at the same time with the same device.

The TOF-tracker concept, the simultaneous measurement of accurate time and bi-dimensional space coordinates in a single gaseous detector, has been previously demonstrated [3] based on Resistive Plate Chamber (RPC) Technology. The detector yielded a time resolution of 77 ps σ along with a bi-dimensional position resolution of 38 μm σ over a full active area of $60 \times 60\,\mathrm{mm}^2$. In this study, it is reported the performance of a large area ($1550 \times 1250\,\mathrm{mm}^2$) TOF-tracker device, with potential to be used for particle identification in High Energy Physics Experiments.

2 Experimental setup

A plastic (poly-methyl methacrylate, PMMA) gas tight box (cassete), see figure 1.a, equipped with feed-throughs for gas and High Voltage (HV) connections, encloses and confines the gas gaps, the glass and the HV electrodes. Inside this box, a multi-gap RPC structure [4] with four gas gaps is

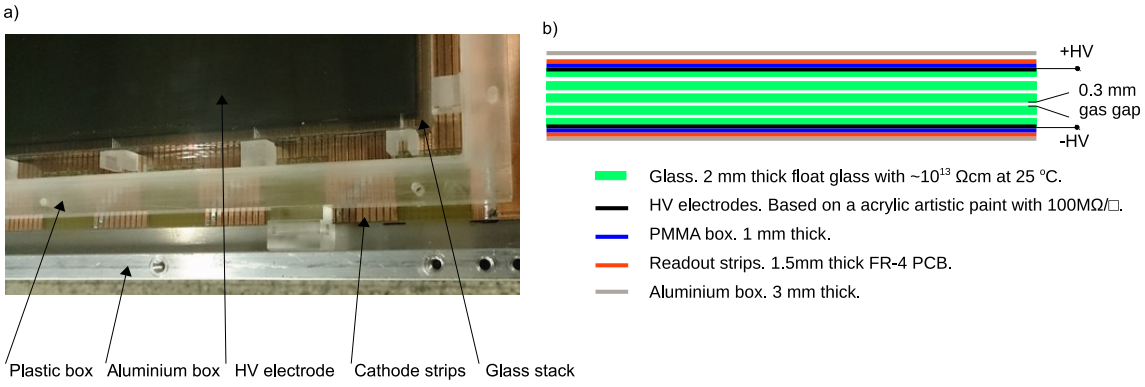

Figure 1. a) Cassette consisting of a plastic tight box, which encloses and confines the gas gaps and the glass and high voltage electrodes and b) sketch of the inner structure of the chamber.

defined by five 2 mm thick float glass[1] electrodes of about $1550 \times 1250\,\mathrm{mm}^2$ separated by 0.3 mm nylon mono-filaments. The HV electrodes are made up of a resistive layer[2] applied to the outer surface of the outermost glasses with airbrush techniques. A sketch of the inner structure of the chamber is shown in figure 1.b. The multi-gap RPC was operated in pure $C_2H_2F_4$ in open gas flow.

Signals are induced both in anode and cathode pick-up electrodes placed directly above and below the cassette. These are made from standard 1.5 mm thick FR-4 Printed Circuit Board (PCB).

Anode signals are induced in 2.5 mm pitch metallic strips (2.1 mm width) placed along the largest dimension, longitudinal dimension, Y, see figure 2. Strips are grouped in sixteen groups of thirty one strips each. All the strips of each group are connected in parallel at both ends to custom timing circuits [5] in order to provide the time, T_i, and the coarse longitudinal position Y_{c_i} as:

$$T_i = \frac{1}{2}(T_{f_i} + T_{b_i}), \tag{2.1a}$$

$$Y_{c_i} = \frac{v_p}{2}(T_{f_i} - T_{b_i}) \tag{2.1b}$$

where T_{f_i} and T_{b_i} are the time measured in front and back sides of each group i, respectively, and v_p the signal propagation velocity in the detector, with a value of around 200 mm/ns. In addition, all the strips within a group are connected through a signal division network to charge sensing amplifiers in order to provide the transversal position, X, as:

$$X = \frac{Q_{al_i} - Q_{ar_i}}{Q_{al_i} + Q_{ar_i}} + x_{g_i} = x_i + x_{g_i} \quad i = 1 \ldots 16 \tag{2.2}$$

where Q_{al_i} and Q_{ar_i} are the anode charge, readout in left and right side of the signal division network, respectively, for the group i and x_{g_i} is the physical position of the group i (i can go from one to sixteen and corresponds to the group with the highest charge). Signals Q_{al_i} and $Q_{ar_{i+1}}$ are connected to the same charge sensing amplifier, therefore the readout of the anode signals comprise in total, seventeen channels/layer. The total charge induced in the anode is defined as: $Q_{a_i} = Q_{al_i} + Q_{ar_i}$.

[1] Bulk resistivity of approximately 10^{13} Ωcm at 25°C.

[2] Based on an artistic acrylic paint with around 100 MΩ/□.

2016 JINST 11 C10002

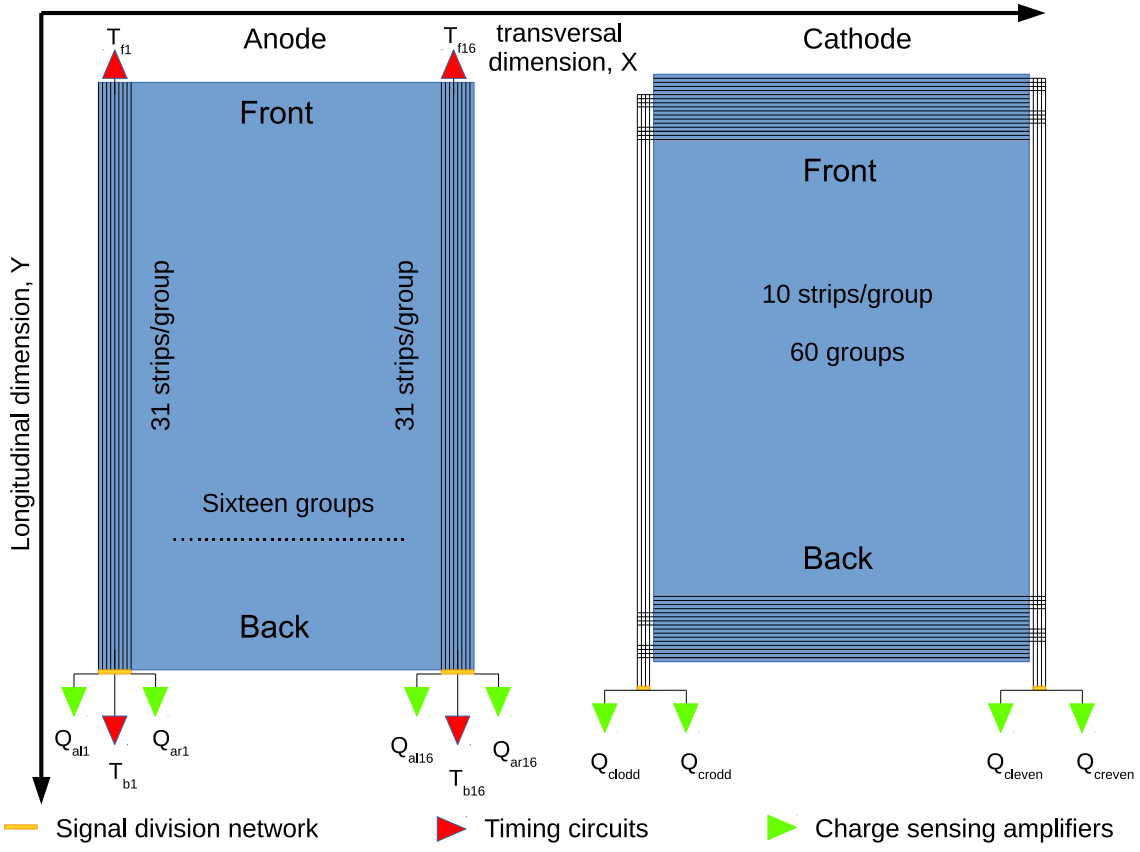

Figure 2. Schematic of the anode and cathode pick-up electrodes, based on 2.5 mm pitch metallic strips.

Cathode signals also are induced in 2.5 mm pitch metallic strips (2.1 mm width) placed along the shortest dimension, transversal dimension, X, see figure 2. Strips are grouped in 60 groups of ten strips each. Odd groups, nicknamed as odd section, (similar strategy is adopted for even groups) are connected all together in parallel to a signal division network and this to charge sensing amplifiers in order to provide the longitudinal position, Y, as:

$$Y = \frac{Q_{cl_j} - Q_{cr_j}}{Q_{cl_j} + Q_{cr_j}} + y_{g_j} = y_j + y_{g_j} \quad j = \text{odd, even} \tag{2.3}$$

where Q_{cl_j} and Q_{cr_j}, are the cathode charge, readout in left and right side of the signal division network, respectively, for the section j (j can refer to odd or even sections and corresponds to the section with highest charge). The physical position of the group with signal is indicated by y_{g_j}. The existing ambiguity within a section (30 groups area connected in parallel) is disentangled using the Y_c variable, which indicates which group produces a signal within a section. The total charge induced in the cathode is defined as: $Q_{c_j} = Q_{cl_j} + Q_{cr_j}$.

The outputs of the charge sensing amplifiers are digitized by 40 MHz streaming ADCs (AD9219) and digitally filtered in the time domain by a trapezoidal filter. The outputs of every eight timing circuits are wired-or together (four channels/layer in total) and send to a FPGA based TDC with a time resolution of 20 ps. Further details on the data acquisition system based on

2016 JINST 11 C10002

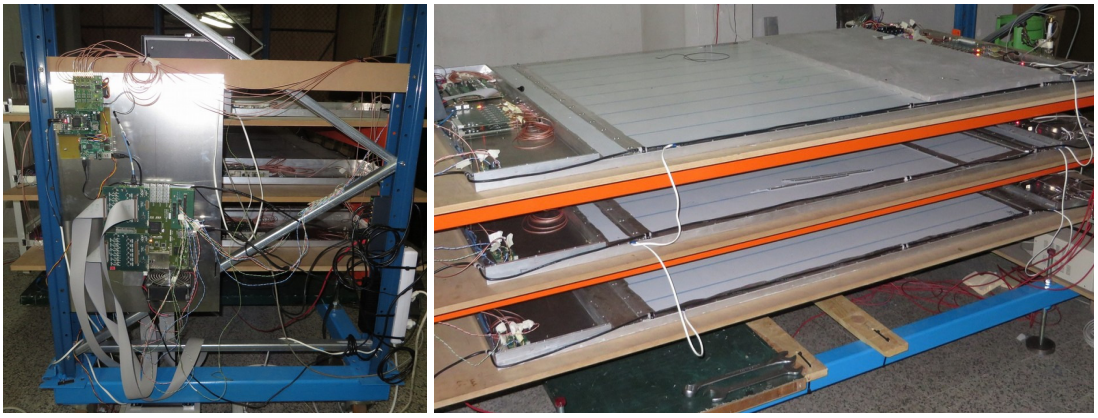

Figure 3. Detailed view of the DAQ board, TRB3, used to readout the entire system (left) and lateral view of the telescope consisting on three identical layers (right).

the TRB3 platform can be found in [6, 7]. The readout of the detector comprises twenty one charge sensing amplifiers and thirty two timing channels on the front end electronics side and twenty one ADC and four TDC channels on the DAQ side.

Three identical layers, L_i $i = 1, 2, 3$, have been stacked vertically, spaced by 225 mm, forming a muon telescope in order to test the performance of the detector, see figure 3. In the following, a superscript, L_i, is added to all variables, that denotes the layer to which refers. The three layer telescope tracked cosmic muons upon a coincidence trigger generated by a majority unit set to level two.

3 Methods

The results presented in these sections are obtained for a selection of events with a longitudinal coarse position, Y_c, within $\pm 700\,mm$ and deposited charge, only in one group of strips in the anode, which should correspond roughly with a single hit in the layer, referred, in the following, as multiplicity one, $M1$.

3.1 Efficiency

The detection efficiency, for a selected sample of events (see below), is calculated for the middle layer, L_2. Two efficiencies are calculated, ε_t and ε_q, computed as the ratio of number of events in L_2 with signal in the timing channels, $\#(T_2)$, and $Q_a^{L_2}$ above a certain threshold, $\#(Q_a^{L_2} > Q_{th})$, respectively, divided by the number of events in the sample, $\#(S)$, therefore,

$$\varepsilon_t = \frac{\#(T_2)}{\#(S)} \qquad \varepsilon_q = \frac{\#(Q_a^{L_2} > Q_{th})}{\#(S)} \tag{3.1}$$

In addition to the requirements described in the beginning of the section, the sample of events fulfils also the requirement of having hits in layer L_1 and L_3 with a time difference, ΔT_{13} within $\pm 3\sigma$ around the average value. As the trigger logic is set to majority of two, the sample of events represents the coincidence between L_1 and L_3.

2016 JINST 11 C10002

3.2 Time resolution

The time resolution, $\sigma(T_i)$, for a given layer L_i is evaluated by characterizing the distributions $\Delta T_{12} = T_1 - T_2$ and $\Delta T_{23} = T_2 - T_3$. In order to characterize the resulting non-gaussian distributions, the standard deviation of a gaussian fit within $\pm 1.5\ \sigma$ around the mean of the original distributions, $\sigma(\Delta T_{ij})$, is calculated. The time resolution, $\sigma(T_i)$, for a given layer, L_i, is simply calculated, assuming same behaviour for each couple of layers, dividing $\sigma(\Delta T_{ij})$ by $\sqrt{2}$.

The distributions ΔT_{ij} are corrected of three effects by using three variables:

- The different muon flight times between layers due to the different flight paths and velocities of the muons, corrected by using ΔT_{13}, the flight time between the external planes in the telescope.

- The different time given by each strip due to the different track length between the end of each strip and the input of the timing circuits, corrected by using the position of the hit inside each group of strips in the anode, x^{L_i} and x^{L_j}, see section 2.

- The influence of the two charges (slewing correction) corrected by using $Q_a^{L_i}$ and $Q_a^{L_j}$.

3.3 Position resolution

A straight-line fit is performed to the three available coordinates in each dimension and the residuals calculated. In order to characterize the resulting non-gaussian distributions, the standard deviation of a gaussian fit within $\pm 1.5\ \sigma$ around the mean of the original distributions is calculated. Since the residuals of three points to a straight-line fit tend to minimize the residuals of the first and third point and maximize the residual of the second, the obtained values are multiplied by the empirical values [3/2 3/4 3/2] in order to equalize the contribution of each layer.

4 Results

4.1 Efficiency

Figure 4.a shows the ϵ_q map for the layer L_2 showing non noticeable dependence with position in the full area of the detector, $1550 \times 1250\,\mathrm{mm}^2$, and an average value of 0.92. Figure 4.b shows ϵ_q and ϵ_t (measured at $V_{th} = 10\,\mathrm{mV}$) as a function of the HV/gap. The flat behaviour of ϵ_q indicates that the detector is operated in the efficiency plateau (this affirmation is also supported by figure 2.d from [8]). The low value of ϵ_q, could suggest the presence of fake muons on the sample, trigger impurity, to be further investigated. The lower value of ϵ_t, 0.72, and the slight increase with HV reveals a lower sensitivity of the timing channels when compared to the charge channels, i.e., part of the signals visible on the charge channels are not visible on the timing channels. This is also visible on figure 4.c where ϵ_t is shown as a function of the threshold on the timing circuits, V_{th}, showing a strong dependence (ϵ_q is plotted for reference). An extrapolation of ϵ_t suggest that the timing channels will provide the same efficiency that the charge channels for a value of V_{th} of around 5 mV.

2016 JINST 11 C10002

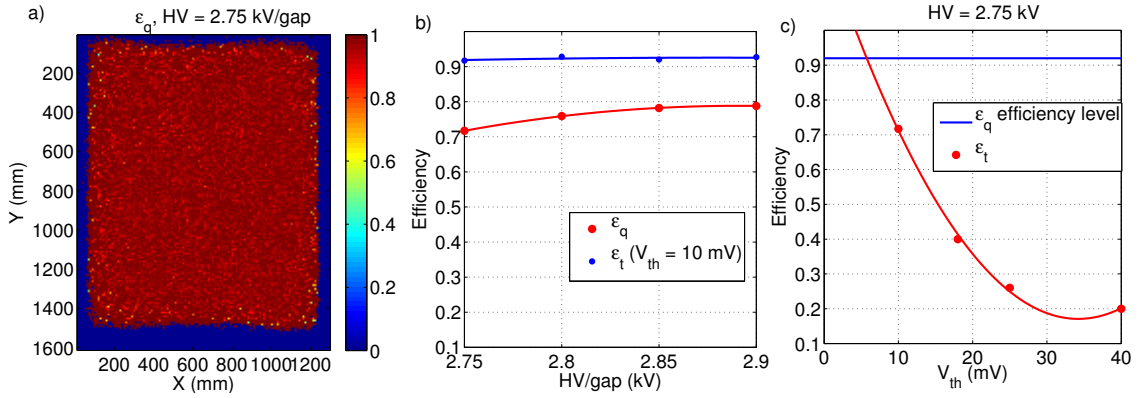

Figure 4. a) ϵ_q map for the layer L_2 showing non noticeable dependence with position in the full area of the detector, $1550 \times 1250\,\mathrm{mm}^2$, and an average value of 0.92. b) and c) ϵ_q and ϵ_t as a function of the HV/gap and threshold on the timing circuits, respectively.

4.2 Time resolution

Figure 5 shows: a) the raw time difference between L_1 and L_2, ΔT_{12}, b) the correlation with ΔT_{13} and its correction function, c) the correlation with x^{L_1} and its correction function (similar behaviour is observed with x^{L_2}), d) the correlation with charge measured in anode, $Q_a^{L_1}$ (similar behaviour is observed with charge $Q_a^{L_2}$) and e) the final time difference after applying all correction. The setting of V_{th} in the timing circuits is 10 mV. The value for $\sigma(\Delta T_{12})$ is around 215 ps, which gives a value of around 152 ps for $\sigma(T_1)$ and $\sigma(T_2)$. Similar behaviour is observer for $\sigma(\Delta T_{23})$ with a value of around 213 ps, which gives a value of around 150 ps for $\sigma(T_2)$ and $\sigma(T_3)$.

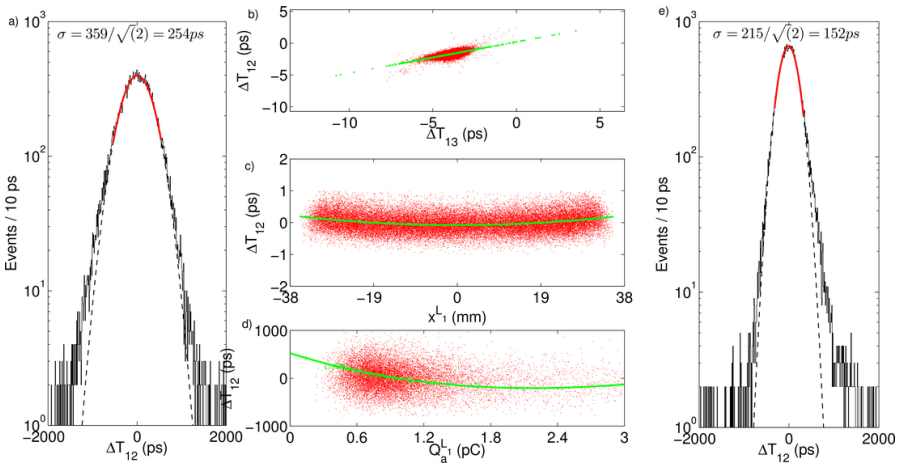

Figure 5. a) Raw time difference ΔT_{12}. b) Correlation with ΔT_{13}. c) Correlation with x^{L_1} (position of the hit inside each group of strips in the anode). d) Correlation with charge measured in anode. e) Final time difference ΔT_{12} after applying all correction. The setting of V_{th} in the timing circuits is 10 mV.

2016 JINST 11 C10002

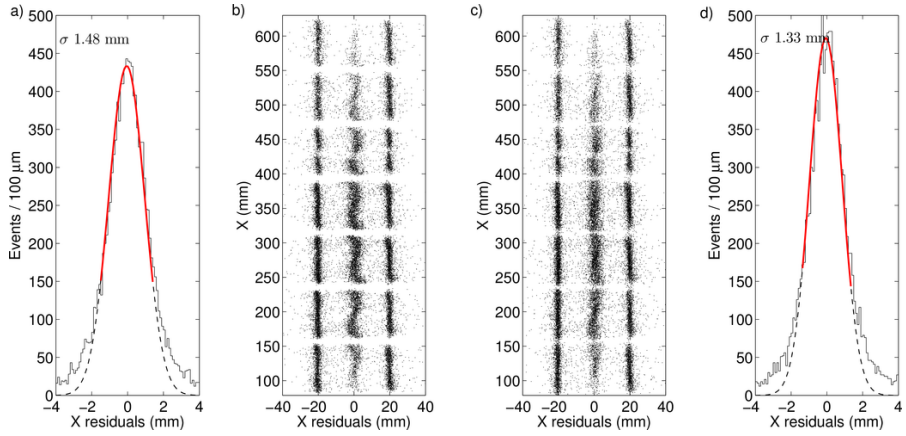

Figure 6. a) Residuals to the straight-line fit to each coordinate of the transversal dimension, X, b) systematic dependence of the residuals on the corresponding coordinate (an offset of ±20 mm has been added to L_1 and L_3 residual, respectively, to help on the visualization c) same as b) but after correction of systematic effects and d) residuals after correction.

4.3 Position resolution

Figure 6 shows: a) residuals to the straight-line fit to each coordinate of the transversal dimension, X, with a width of around 1.48 mm σ, b) dependence of the residuals with the corresponding coordinate, showing some systematic effects, c) same as b) but after correction and d) the residuals after correction with a width of around 1.33 mm σ. Two strategies have been applied in order to correct the observed systematic effects: one is to correct the residuals by using an empirical function obtained by fitting the observed dependence with the corresponding coordinate and the other is to correct the measured position using a curve that relate the measured and real position, which has been obtained by using a test signal injected into different positions of the signal division network. Both approaches deliver similar results, but some systematic effects are still visible. The electronic resolution of the readout has been measured by using a chamber with strips in the same direction on anode and cathode an also using a test signal in the present experimental setup. The result shows a clear sub-millimetre resolution, better than 0.7 mm σ (contribution to the residuals

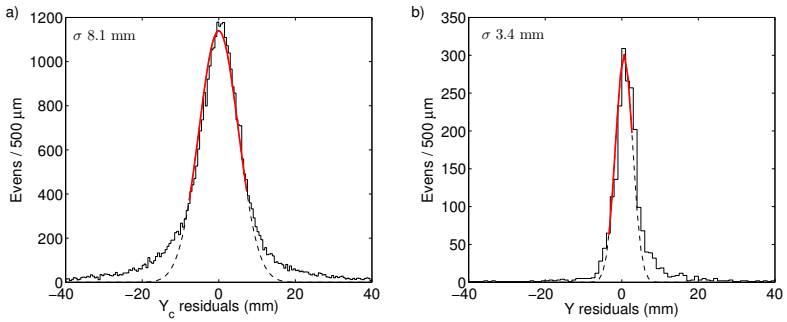

Figure 7. a) Residuals to the straight-line fit to each coordinate of the coarse longitudinal dimension, Y_c and b) residual to each coordinate of the longitudinal dimension, Y.

2016 JINST 11 C10002

0.4 mm σ), suggesting that the measured resolution here reported is strongly affected by other effects like uncorrected systematic effects.

Figure 7 shows: a) residuals to the straight-line fit to each coordinate of the coarse longitudinal dimension, Y_c, with a width of around 8.1 mm σ and b) residual of the longitudinal dimension, Y, with a width of around 3.4 mm σ.

5 Conclusions

Three layers of large area, $1550 \times 1250\,\text{mm}^2$, TOF-tracker devices — RPC detectors capable of measuring time and bi-dimensional position at the same time — have been assembled and tested by tracking cosmic muons. The system is only readout by 53 and 25 channels/layer of FEE and DAQ, respectively.

Each of the three layers yields a position resolution down to 1.33 mm σ, with a contribution of the readout chain of 0.4 mm σ, together with a single layer time resolution of 150 ps σ and an efficiency of 92%, over the entire area of the detector, without significant cuts, a fine alignment procedure or deep systematic effects correction. The efficiency of 92% is achieved on the tracking while in the timing measurement is achieved a value of 72% due to the lack of sensitivity on the timing circuits compared with the charge sensing circuits. This situation will be mitigated by increasing the available signal, reducing the glass thickness or increasing the number of gaps, or by increasing the signal to noise ratio on the timing circuits. All this modifications will be implemented in the next prototype.

Acknowledgments

This work was supported by FCT/COMPETE under the contract CERN/FIS-NUC/0038/2015.

References

[1] C. Lippmann, *Particle identification*, *Nucl. Instrum. Meth.* **A 666** (2012) 148 [arXiv:1101.3276].

[2] W. Klempt, *Review of particle identification by time-of-flight techniques*, *Nucl. Instrum. Meth.* **A 433** (1999) 542.

[3] A. Blanco, P. Fonte, L. Lopes, P. Martins, J. Michel, M. Palka et al., *TOFtracker: Gaseous detector with bidimensional tracking and time-of-flight capabilities*, 2012 *JINST* **7** P11012.

[4] E. Cerron Zeballos, I. Crotty, D. Hatzifotiadou, J. Lamas Valverde, S. Neupane, M.C.S. Williams et al., *A New type of resistive plate chamber: The Multigap RPC*, *Nucl. Instrum. Meth.* **A 374** (1996) 132.

[5] P. Assis, P. Brogueira, M. Ferreira, R. Luz and L. Mendes, *Design and characterization of the PREC (Prototype Readout Electronics for Counting particles)*, 2016 *JINST* **11** T08004.

[6] A. Neiser et al., *TRB3: a 264 channel high precision TDC platform and its applications*, 2013 *JINST* **8** C12043.

[7] http://trb.gsi.de/.

[8] L. Lopes, P. Fonte and A. Mangiarotti, *Systematic study of gas mixtures for timing RPCs*, *Nucl. Instrum. Meth.* **A 661** (2012) S194.

2016 JINST 11 C10002